

pubs.acs.org/biochemistry Article

Leveraging Peptide Sequence Modification to Promote Assembly of Chiral Helical Gold Nanoparticle Superstructures

Soumitra Mokashi-Punekar, Sydney C. Brooks, Camera D. Hogan, and Nathaniel L. Rosi*



Cite This: https://dx.doi.org/10.1021/acs.biochem.0c00361



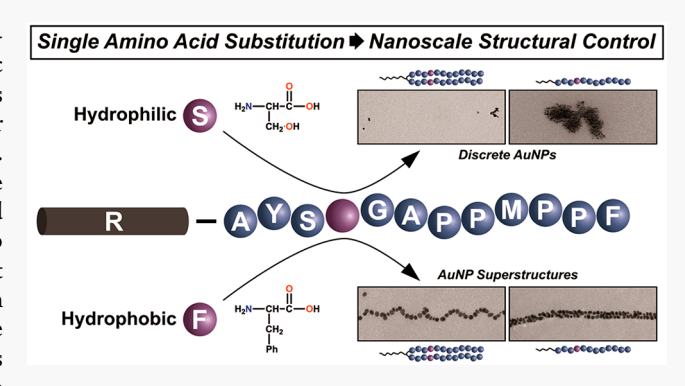
ACCESS

III Metrics & More

Article Recommendations

s Supporting Information

ABSTRACT: Peptide conjugate molecules comprising a gold-binding peptide (e.g., AYSSGAPPMPPF) attached to an aliphatic tail have proven to be powerful agents for directing the synthesis and assembly of gold nanoparticle superstructures, in particular chiral helices having interesting plasmonic chiroptical properties. The composition and structure of these molecular agents can be tailored to carefully tune the structure and properties of gold nanoparticle single and double helices. To date, modifications to the β -sheet region (AYSSGA) of the peptide sequence have not been exploited to control the metrics and assembly of such superstructures. We report here that systematic peptide sequence variation in a series of gold-binding peptide conjugate molecules can be leveraged not only to affect the assembly of peptide



conjugates but also to control the synthesis, assembly, and optical properties of gold nanoparticle superstructures. Depending upon the hydrophobicity of a single-amino acid variant, the conjugates yield either dispersed gold nanoparticles or helical superstructures. These results provide evidence that subtle changes to peptide sequence, via single-amino acid variation in the β -sheet region, can be leveraged to program structural control in chiral gold nanoparticle superstructures.

Plasmonic metal nanoparticles (NPs) are important building blocks for constructing a wide variety of materials whose properties depend not only on the size, shape, and composition of the component NPs but also on their precise arrangement in three-dimensional (3D) space. 1-4 Helical NP superstructures have attracted widespread interest because they exhibit strong plasmonic chiroptical activity, 5-7 which makes them attractive for a range of potential applications.^{8,9} Their plasmonic chiroptical response derives from the intrinsic chiral 3D arrangement of the component NPs, and the intensity of the response depends largely on metrics such as helical pitch length and NP dimensions, with the strongest chiroptical signal predicted to arise from helices with a short pitch and large NPs. 10,11 The rational construction and systematic structure and property optimization of helical NP superstructures, and NP superstructures in general, require robust assembly platforms. To this end, we have developed a peptide-based platform for assembling NPs into structurally complex architectures. 12-21 Much of our research has focused on using this peptide platform to design and construct chiral, helical NP assemblies, in particular gold (Au) NP-based single^{20–23} and double helices. ^{12,14,17,19}

Our assembly strategy is based on peptide conjugates, which are molecular agents consisting of an organic tail appended to a NP-binding peptide. When a given peptide conjugate is dissolved in an aqueous assembly buffer along with appropriate inorganic salts and reducing agents, it directs the synthesis and

assembly of inorganic NPs; NP nucleation/growth and assembly are coincident processes. 12,15 Here, we restrict our discussion to Au-binding peptide conjugates of the general formulas C_x -(PEP_{Au})_v (PEP_{Au} = AYSSGAPPMPPF; also known as A3²⁴), which feature prominently in this study. An individual Au-binding peptide conjugate can be subdivided into multiple sections that each play a key role in the assembly process. First, each peptide conjugate has an aliphatic tail (C_x) appended to the N-terminus of PEPAu. The aliphatic tail helps drive peptide conjugate aggregation in aqueous assembly media and plays a key role in dictating the morphology of the target assembly. 12,13,25 Second, the six N-terminal amino acids of PEPAW AYSSGA, which are adjacent to the aliphatic tail, also play an important role in peptide conjugate assembly. Specifically, they engage in interpeptide β -sheet formation, which helps direct the assembly of peptide conjugates into chiral fibers, including helical coils and twisted ribbons. 12,20 The third and final section consists of the C-terminal amino acids, PPMPPF. This region of PEPAu adopts a PPII

Special Issue: Biochemistry at the Nanoscale

Received: April 30, 2020 Revised: June 3, 2020 Published: June 8, 2020



conformation, ^{20,26} and experimental and computational studies indicate that this region strongly associates with AuNP surfaces. ^{20,23,27}

In the context of building and optimizing the chiroptical properties of helical NP superstructures, we have successfully demonstrated that (i) the global molecular structure and composition of the peptide conjugates can be modified to direct formation of either single or double helices, 12,17-20 (ii) varying the amino acid sequence within the PPII region profoundly affects the dimensions of the component AuNPs in single-helix superstructures, 23 and (iii) a small adjustment of the aliphatic tail length can lead to dramatic changes in the length of the helical pitch of these assemblies. 19,22 For the latter, we specifically reported that C_x -(PEP_{Au}^{M-ox})₂ (x = 16-22, and M-ox is the oxidized form of methionine) assembles into helical ribbon fibers in HEPES buffer, such that the ribbon width and helical pitch increase with an increase in aliphatic tail length.²² This effect translates to the final AuNP single helices: C_{16-22} -(PEP_{Au}^{M-ox})₂ directs the assembly of singlehelical superstructures ranging in average pitch value from 80 to 120 nm. Contrary to the observed trend, C₁₄-(PEP_{Au} M-ox)₂, when subjected to similar NP superstructure synthesis and assembly conditions, did not assemble into helical fibers and consequently yielded only free unassembled AuNPs.²² We reason that C_{14} -(PEP_{Au} M-ox)₂ exhibits a diminished assembly propensity because of its shorter (less hydrophobic) aliphatic tail. To further decrease the pitch within this family of helices and ultimately increase the magnitude of the plasmonic chiroptical signal, we must identify an alternate strategy for promoting the assembly of peptide conjugates with aliphatic tails shorter than C₁₆. In this study, we examine for the first time whether modifications to the β -sheet-forming region of PEP_{Au} affect peptide conjugate assembly, potentially providing yet another synthetic handle for tuning the metrics and properties of helical NP superstructures.

■ EXPERIMENTAL METHODS

General Methods and Materials. All chemicals were obtained from commercial sources and used without further purification. All peptides were synthesized using established microwave-assisted solid phase peptide synthesis protocols on a CEM Mars microwave. Nanopure water (18.1 m Ω) from a Barnstead Diamond water purification system was used to prepare all aqueous solutions. Peptides were purified by reverse phase high-performance liquid chromatography on an Agilent 1200 liquid chromatographic system equipped with diode array and multiple-wavelength detectors using a Zorbax-300SB C₁₈ column. Peptide masses were confirmed by liquid chromatography-mass spectrometry (LC-MS) data using a Shimadzu LC-MS 2020 instrument. Ultraviolet-visible (UV-vis) spectra were recorded using an Agilent 8453 UV-vis spectrometer with a quartz cuvette (10 mm path length). All microscopy measurements were performed using ImageJ.

Synthesis. Peptide Synthesis. The peptides used in this work were synthesized via an established microwave-assisted solid phase peptide synthesis protocol. In summary, 138.8 mg (0.25 mmol) of Fmoc-Phe-Novasyn TGA resin (Millipore catalog no. 8560340001) swelled in dimethylformamide (DMF) for 15 min. The Fmoc-Phe-Novasyn TGA resin was deprotected by adding 2 mL of 20% 4-methylpiperidine in DMF to the resin, heating the mixture to 75 °C in 1 min, and maintaining that temperature for an additional 2 min. A filtration manifold was used to drain excess reagent, and the

resin was then washed with 3 × 5 mL of DMF. For the coupling step, a 0.1 M solution of HCTU in NMP (5 equiv, 1.25 mL) and DIEA (7 equiv, 0.175 mmol, 30.4 μ L) were added to Fmoc-protected amino acid (4 equiv, 0.125 mmol). The solution was then thoroughly vortexed and centrifuged to dissolve the amino acid. The resulting solution was added to the washed resin, and the mixture was heated to 75 °C over the course of 1 min and held at that temperature for 5 min. After the coupling step, the excess reagent was drained and the resin was washed with 3 × 5 mL of DMF. This cycle was then repeated for every amino acid. Double coupling of proline and adjacent amino acids was used to ensure the complete reaction of the secondary amide group. For divalent peptide conjugates, the N-terminus was completed by a 5-azido pentanoic acid cap using the same coupling steps described above. For the monovalent peptide conjugates, the final amino acid was deprotected to yield an N-terminal amino group using a previously described deprotection protocol. To produce peptides with the oxidized methionine residue, N₃-PEP_{A11} was dissolved in a 1:1 Nanopure water/acetonitrile solution. A concentrated hydrogen peroxide (H₂O₂) solution was added until the final H₂O₂ concentration was 100 mM. This solution was left undisturbed overnight, and the resulting oxidized product was purified via high-performance liquid chromatography.

Peptide Conjugate Synthesis. The divalent peptide conjugate was synthesized using established protocols. 19,20 C_{14} -dialkyne was attached to each azido peptide sequence via Cu-catalyzed click chemistry described previously. The monovalent peptide conjugate was synthesized by following a previously reported protocol, coupling succinimide-activated decanoic acid (C_{10} -NHS) to the free N-terminus of the peptide sequence. 12

Assembly Conditions. Peptide Conjugate Assembly. To the lyophilized peptide conjugate (18.725 nmol for single-helix peptide conjugates and 74.9 nmol for double-helix peptide conjugates) was added 250 μ L of 0.1 M HEPES buffer. The solution was sonicated for 5 min and then left undisturbed at room temperature for approximately 16 h before TEM sample preparation.

Assembly of AuNP Single Helices. First, 18.725 nmol of C_{14} -(PEP_{Au} M-ox)₂ (X = S, T, or F) was dissolved in 250 μ L of 0.1 M HEPES buffer, sonicated for 5 min, and then left undisturbed for 25 min. Next, 2 μ L of a 1:1 mixture of aqueous 0.1 M HAuCl₄ in 1 M TEAA buffer was added to the peptide conjugate solution. Approximately 2–3 s after addition of a gold precursor solution, a black precipitate appeared. The vial was vortexed immediately after the appearance of the precipitate.

Assembly of AuNP Double Helices. First, 74.9 nmol of C_{10} -PEP $_{Au}^{\ \ X}$ (X = S, T, or F) was dissolved in 250 μ L of 0.1 M HEPES buffer and allowed to sit undisturbed for 30 min. A solution of 0.1 M HAuCl $_4$ in 0.1 M TEAA buffer was prepared and allowed to sit for 10 min, and then a 100 μ L aliquot was transferred to a new vial and centrifuged for 10 min at 10 rpm. Two microliters of this solution was added to the peptide conjugate solution. Upon appearance of a black precipitate, the vial was immediately vortexed.

Characterization and Sample Preparation. Circular Dichroism (CD) Spectroscopy. CD measurements were collected with an Olis DSM 17 CD spectrometer with a quartz cuvette (0.1 cm path length) at 25 $^{\circ}$ C with a scan rate of 8 nm/min. Solutions in 10 mM HEPES buffer for C₁₄-

 $(PEP_{Au}^{Mox})_2^X$ (75 μ M) or C_{10} -PEP_{Au} (300 μ M) were prepared for each CD measurement (X = S, T, or F).

Attenuated Total Reflectance Fourier Transform Infrared Spectroscopy (ATR-FTIR). ATR-FTIR measurements were collected with a PerkinElmer Spectrum 100 FTIR instrument equipped with an ATR accessory and recorded with PerkinElmer Spectrum Express software. C_{14} -(PEP $_{Au}^{Mox}$) $_{2}^{X}$ (75 μ M) or C_{10} -PEP $_{Au}^{X}$ (300 μ M) in 0.1 M HEPES buffer was prepared and left undisturbed on the benchtop for ~24 h (X = S, T, or F). The solution was then dialyzed against Nanopure water using d-tube dialyzers (Millipore catalog no. 71505-3). After dialysis, the peptide conjugate solution was concentrated via evaporation and was drop cast onto the ATR substrate prior to data collection.

Atomic Force Microscopy (AFM). AFM measurements were collected in tapping mode using the Asylum MFP-3D atomic force microscope and ultrasharp AFM tips (NanoandMore SHR-150). A 0.1% APTES (3-aminopropyl-triethoxy-silane) solution was drop casted onto a freshly cut mica surface, and then the surface was rinsed with Nanopure water; 50 μ L of C₁₄-(PEP_{Au}^{Mox})₂^F (75 μ M) or C₁₀-PEP_{Au}^F (300 μ M) in 0.1 M HEPES was then drop cast and rinsed with water after 1 min and allowed to dry in the desiccator overnight.

Transmission Electron Microscopy (TEM). TEM was conducted on a FEI Morgagni 268 instrument operated at 80 kV and equipped with an AMT side mount CCD camera system. Six microliters of 50 μ L of C₁₄-(PEP_{Au}^{Mox})₂^X (75 μ M) or C₁₀-PEP_{Au}^X (300 μ M) in 0.1 M HEPES was drop cast onto a 3 mm diameter copper grid with Formvar coating (X = S, T, or F). After 5 min, excess solution was wicked away and the grid air-dried for 2 min. For studying peptide conjugate assembly, 6 μ L of phosphotungstic acid (pH 7) was drop cast onto the grid and allowed to sit for 30 s. For studying nanoparticle assemblies, 6 μ L of Nanopure water was drop cast onto the grid and allowed to sit for 30 s. Excess solution was wicked away, and the grid air-dried for 5 min.

RESULTS AND DISCUSSION

We designed a series of sequence-modified C₁₄-(PEP_{Au}^{M-ox})₂ peptide conjugates having incrementally increasing relative hydrophobicity in their β -sheet-forming region to promote fiber and superstructure assembly (Figure 1). Because the β sheet-forming residues (-AYSSGA) are not associated with gold binding in the proposed assembly model,²⁰ we hypothesize that replacing the hydrophilic S residue with more hydrophobic amino acids will effectively increase the hydrophobic to hydrophilic ratio in C_{14} - $(PEP_{Au}^{M-ox})_2$ without detrimentally affecting NP binding. To test this hypothesis, we synthesized two new backbone-modified peptide conjugates: C_{14} -(AYSXGAPPM^{ox}PPF)₂, where X = T or F (Figures S1 and S2). Hereafter, each peptide conjugate is referenced by its modified amino acid residue: C₁₄-(AYSFGAPPM^{ox}PPF)₂ = C_{14} - $(PEP_{Au}^{M-ox})_2^F$. Our established model for C_{18} - $(PEP_{Au}^{M-ox})_2$ assembly 20 guided our decision to substitute at the fourth position. According to this model, there are two different interfaces between the stacked β -sheets: an aromatic interface defined by the Y (position 2) and S (position 4) side chains (~9 Å distance between stacked β -sheets) and an interface defined by the A (position 1) and S (position 3) side chains (\sim 6.5 Å distance between stacked β -sheets). Because the larger Y-S interface is dictated by the steric bulk of Y, we reasoned that replacing the S at the fourth position with larger, more hydrophobic residues (T or F) would not significantly disrupt

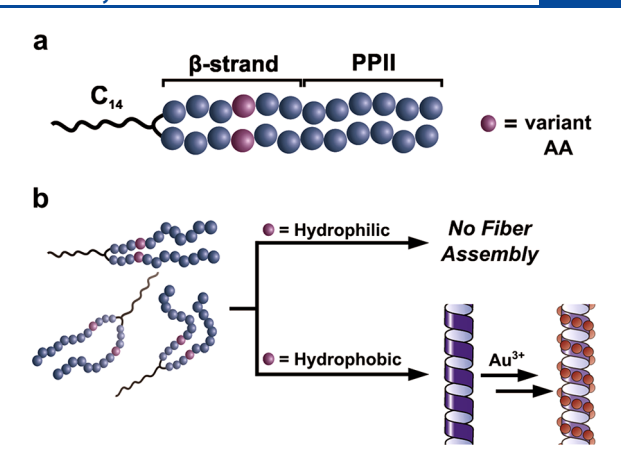


Figure 1. Peptide conjugate design and β-sheet modification strategy for C_{14} -(PEP_{Au}^{M-ox})₂. (a) Peptide conjugates contain a C_{14} aliphatic tail attached to the N-terminus of the peptide, which has a β-sheet-forming region and an inorganic particle-binding region (PPII section). (b) The fourth amino acid in the sequence will be replaced with increasingly hydrophobic amino acids, which are expected to increase the assembly propensity of the peptide conjugate and thereby promote the assembly of AuNP superstructures.

 β -sheet stacking. We note that similar peptide sequence modifications have been shown to significantly affect peptide assembly. Stupp et al. reported that the morphology of one-dimensional (1D) fibers derived from a family of peptide conjugates can vary on the basis of the relative position of hydrophilic and hydrophobic amino acids, ²⁸ and Stevens et al. showed that minute backbone changes, such as S to T substitution, can alter peptide fiber morphology from twisted to planar ribbons. ²⁹

We dissolved each conjugate in 0.1 M HEPES buffer [4-(2hydroxyethyl)-1-piperazineethanesulfonic acid] (pH 7.3) at room temperature and examined their resulting assemblies using TEM. Images of negatively stained samples revealed that only C_{14} -(PEP_{Au}^{M-ox})₂^F assembles into 1D fibers, while C_{14} -(PEP_{Au}^{M-ox})₂^S and C_{14} -(PEP_{Au}^{M-ox})₂^T do not assemble into any well-defined structures (Figure 2a,b and Figure S3). CD spectroscopy and FTIR spectroscopy were used to determine the peptide secondary structure. ³⁰ CD spectra of C_{14} -(PEP_{Au} $^{M-ox}$)₂ display characteristic β -sheet signals at \sim 215–220 nm, 20,22,30,31 while spectra of C_{14} -(PEP_{Au} $^{M-ox}$)₂ and C_{14} -(PEP_{Au} $^{M-ox}$)₂ reveal peaks at \sim 205 nm, which is indicative of C_{14} -(PEP_{Au} $^{M-ox}$)₂ reveal peaks at C_{14} -(PEP_{Au} $^{M-ox}$)₃ reveal peaks at C_{14} -(PEP_{Au} $^{M-ox}$)₄ reveal peaks at C_{14} -(PEP_{Au} $^{M-ox}$)₅ reveal peaks at C_{14} -(PEP_{Au} $^{M-ox}$)₆ reveal peaks at C_{14} -(PEP_{Au} $^{M-ox}$)₇ reveal peaks at C_{14} -(PEP_{Au} $^{M-ox}$)₈ reveal peaks at C_{14} -(PEP_{Au} $^{M-ox}$)₉ reveal peaks at C_{14} -(PEP_{Au} $^{M-ox}$)₁ reveal peaks at C_{14} -(PEP_{Au} $^{M-ox}$)₂ reveal peaks at C_{14} -(PE unassembled structures in solution (Figure 2c). 20,22,32,33 Similarly, FTIR spectra of C_{14} -(PEP_{Au}^{M-ox})₂^F have distinct amide I peaks centered at ~1630 cm⁻¹ indicative of β -sheet secondary structure,³⁴ while C_{14} -(PEP_{Au}^{M-ox})₂^T and C_{14} -(PEP_{Au}^{M-ox})₂^S display broad peaks centered around ~1645 cm⁻¹, characteristic of unordered structure (Figure 2d).^{20,22,34} Taken together, both microscopic and spectroscopic data are in good agreement and indicate that C_{14} - $(PEP_{Au}^{M-ox})_2^F$ assembles into fibers. We examined the fiber morphology using AFM, which revealed tightly coiled helical ribbons with an average ribbon width of ~28 nm and an average helical pitch of \sim 65 nm (Figure 2e,f and Figures S4 and S5). We note that both the ribbon width and the pitch are significantly shorter than what we observed for C_{16} -(PEP_{Au}^{M-ox})₂ (~47 and ~82 nm, respectively). Collectively, the microscopy and spectroscopy data indicate that modification of the β -sheet region of PEPAu can significantly affect peptide conjugate assembly behavior.

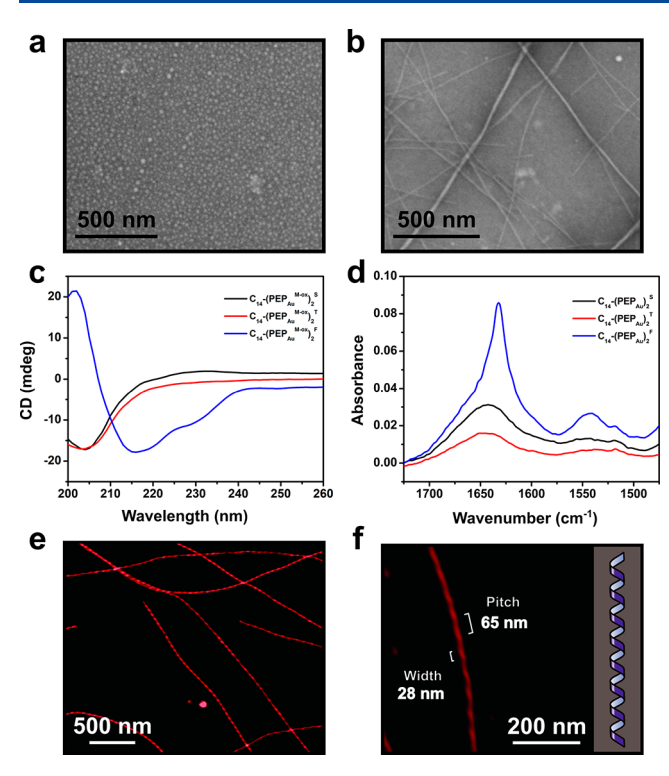


Figure 2. Negatively stained TEM images of (a) C_{14} -(PEP_{Au}^{M-ox})₂^T and (b) C_{14} -(PEP_{Au}^{M-ox})₂^F assemblies. (c) CD and (d) FTIR spectra of C_{14} -(PEP_{Au}^{M-ox})₂^X assemblies. (e) Low- and (f) high-magnification AFM images of C_{14} -(PEP_{Au}^{M-ox})₂^F fibers.

To investigate whether trends in the assembly behavior of the modified peptide conjugates translated to similar patterns in NP assembly, we subjected each sequence-modified peptide conjugate to our established superstructure assembly conditions. As previously discussed, C_{14} -(PEP $_{Au}^{M-ox}$) $_2^{T}$ yielded discrete AuNPs (Figure S6). C_{14} -(PEP $_{Au}^{M-ox}$) $_2^{T}$ also yields discrete NPs, which is consistent with our observation that C_{14} -(PEP $_{Au}^{M-ox}$) $_2^{T}$ does not assemble (Figure 3a). However,

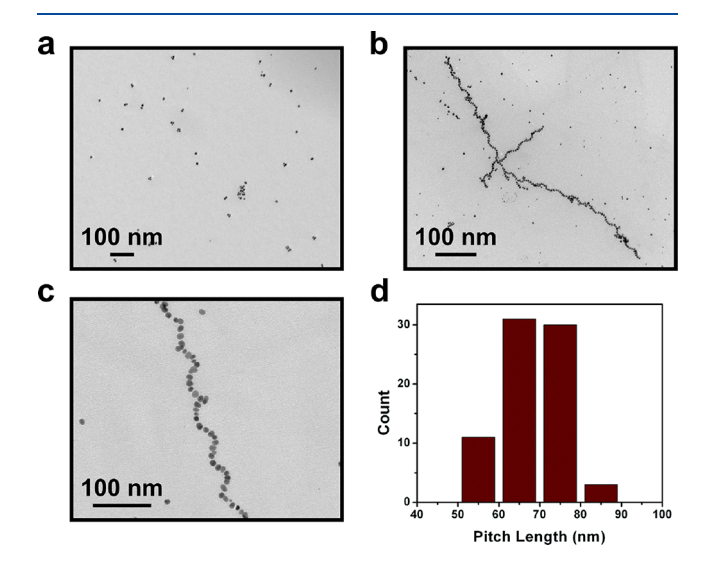


Figure 3. AuNP assemblies formed using backbone-modified peptide conjugates. (a) C_{14} -(PEP_{Au} $^{M-ox}$)₂ T results in discrete unassembled AuNPs. (b and c) C_{14} -(PEP_{Au} $^{M-ox}$)₂ F directs the assembly of AuNP single helices. (d) Helical pitch distribution of single helices derived from C_{14} -(PEP_{Au} $^{M-ox}$)₂ F .

C₁₄-(PEP_{Au}^{M-ox})₂^F yields well-defined AuNP single helices (Figure 3b,c and Figure S7). The average helical pitch is ~67 nm (Figure 3d), which is in agreement with the helical pitch observed for C_{14} -(PEP_{Au}^{M-ox})₂^F helical fibers. The NPs comprising the single helices have an average length and an average width of 11.4 \pm 2.1 and 7.2 \pm 2.3 nm, respectively (Figure S8). As described in our prior studies, the oblong shape of the AuNPs can be attributed to the oxidized methionine residue within the peptide sequence.²³ Importantly, single helices derived from C_{14} - $(PEP_{Au}^{M-ox})_2^F$ exhibit a distinct chiroptical response that is not observed for the products of the C_{14} - $(PEP_{Au}^{M-ox})_2^S$ - and C_{14} - $(PEP_{Au}^{M-ox})_2^T$ based reactions (Figure S9). We note, however, that the chiroptical signal intensity may be further optimized by improving the product yield. Nevertheless, these results represent a significant advance in this methodology: acute molecular modifications to the β -sheet region of the peptide conjugates manifest on the nanoscale in the assembly of helical superstructures.

Encouraged by these results, we turned our attention to a family of double-helical superstructures prepared using C_x -PEP_{Au} conjugates. 12,14,17 We previously reported that C_{12} -PEP_{An} assembles into twisted fibers and directs the assembly of AuNP double helices exhibiting a regular pitch of \sim 85 nm. 12 Attempts to decrease the pitch by shortening the aliphatic tail were unsuccessful, because C₁₀-PEP_{Au}, like C₁₄-(PEP_{Au} M-ox)₂, does not assemble into fibers in aqueous HEPES buffer. We predicted that the β -sheet modification strategy again could be leveraged to produce new peptide conjugates that would form fibers and subsequently direct the assembly of AuNP double helices. To test this prediction, a similar series of peptide conjugates were synthesized: C₁₀-AYSXGAPPMPPF, where X = T or F [C_{10} -PEP $_{Au}^{T}$ and C_{10} -PEP $_{Au}^{F}$ (Figures S10 and S11)]. When dissolved in 0.1 M HEPES, only the most hydrophobic peptide conjugate, C₁₀-PEP_{Au}^F, assembles into fibers (Figure 4a and Figure S12), as determined via TEM imaging. A negative band at ~220 nm in the CD spectrum and an amide I peak at ~1630 cm⁻¹ in the FTIR spectrum of the assembled fibers (Figure 4b,c) are attributed to the presence of β -sheet secondary structure, which is consistent with our previous studies. 12 In contrast, CD and FTIR spectra of C_{10} -PEP $_{Au}$ ^S and C_{10} -PEP_{Au} show no evidence of β -sheet structure. C_{12} -PEP_{Au} assembles into fibers that resemble twisted ribbons, 12 and we predicted that C₁₀-PEP_{Au}^F fibers would adopt a similar morphology. However, AFM imaging of the C₁₀-PEP_{Au} fibers does not reveal a discernible morphology (Figure 4d and Figure S13).

We proceeded to investigate whether these modified peptide conjugates could direct the assembly of AuNP superstructures. $C_{10}\text{-PEP}_{Au}^{S}$ and $C_{10}\text{-PEP}_{Au}^{T}$ yield AuNP particles and aggregates, as predicted on the basis of the fact that neither assembled into fibers (Figure S14). $C_{10}\text{-PEP}_{Au}^{F}$, however, directs the assembly of 1D NP assemblies (Figure 4e and Figure S15). Although the superstructures are not as well-defined as the pristine double helices produced using C_{12} -PEP $_{Au}^{12,14,17}$ they do contain distinct double-helical regions, from which an average pitch of 68.5 \pm 13.8 nm was determined. The particles within the superstructures have an average length and an average width of 8.6 \pm 1.5 and 9.4 \pm 1.8 nm, respectively (Figure S16). These particles are more spherical than those in the single helices, because in this case, the methionine is not oxidized.

Biochemistry pubs.acs.org/biochemistry Article

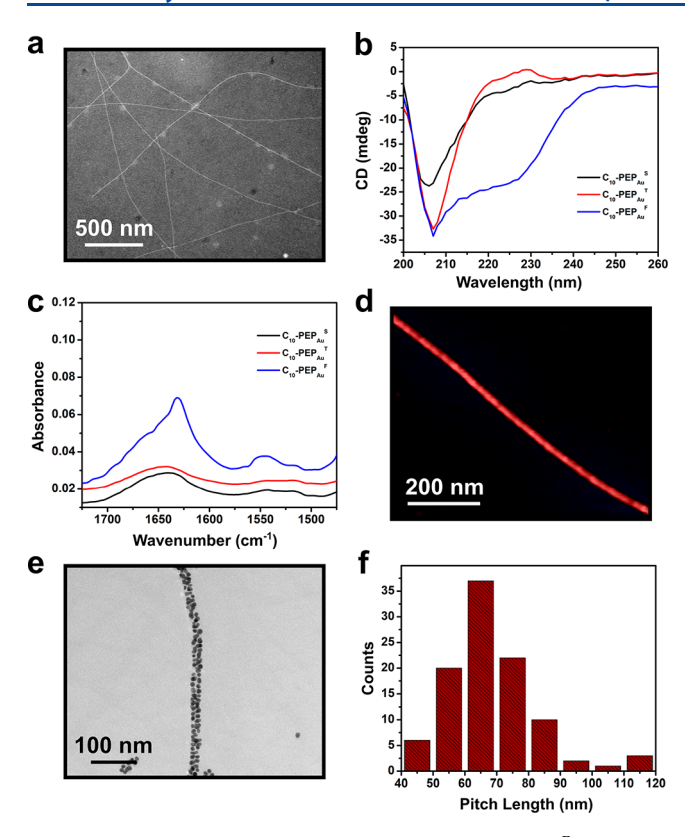


Figure 4. (a) Negatively stained TEM image of C_{10} -PEP_{Au}^F fibers. (b) FTIR and (c) CD spectroscopy of C_{10} -PEP_{Au}^X assemblies. (d) AFM of C_{10} -PEP_{Au}^F fibers. (e) TEM image of AuNP superstructure assembly formed using C_{10} -PEP_{Au}^F and (f) helical pitch distribution of C_{10} -PEP_{Au}^F-based superstructures.

These results successfully demonstrate that an identical set of amino acid modifications can be applied to construct two different chiral architectures: AuNP single helices and AuNP double helices. In both cases, the assembly propensity of peptide conjugates with shorter aliphatic tails can be increased by substituting hydrophilic S with hydrophobic F. Therefore, this amino acid substitution strategy is a powerful and generalizable approach for programming the assembly of chiral AuNP superstructures.

CONCLUSIONS

In this report, we demonstrate that single-amino acid modifications can promote the assembly of two different peptide conjugates into fibers of varying morphologies. We then use these designed peptide conjugate variants to construct chiral superstructures, including AuNP single helices that exhibit a distinct chiroptical response. To fully realize the promise of these new materials, future synthetic optimization is necessary to increase the superstructure yield and maximize the chiroptical signal. More generally, our studies show that synthetically modifying the β -sheet region of these goldbinding peptide conjugates allows for further increased control over NP assembly and that molecular chemistry can be used to dramatically influence nanomaterial design. In the future, we intend to further investigate this relationship through expanded studies that specifically examine the effects of amino acid steric bulk and charge.

ASSOCIATED CONTENT

Supporting Information

The Supporting Information is available free of charge at https://pubs.acs.org/doi/10.1021/acs.biochem.0c00361.

LC-MS, AFM, and TEM data (PDF)

AUTHOR INFORMATION

Corresponding Author

Nathaniel L. Rosi — Department of Chemistry and Department of Chemical and Petroleum Engineering, University of Pittsburgh, Pittsburgh, Pennsylvania 15260, United States;
orcid.org/0000-0001-8025-8906; Email: nrosi@pitt.edu

Authors

Soumitra Mokashi-Punekar — Department of Chemistry, University of Pittsburgh, Pittsburgh, Pennsylvania 15260, United States; o orcid.org/0000-0002-4322-4421

Sydney C. Brooks — Department of Chemistry, University of Pittsburgh, Pittsburgh, Pennsylvania 15260, United States Camera D. Hogan — Department of Chemistry, University of

Pittsburgh, Pittsburgh, Pennsylvania 15260, United States

Complete contact information is available at: https://pubs.acs.org/10.1021/acs.biochem.0c00361

Author Contributions

§S.M.-P. and S.C.B. contributed equally to this work.

Funding

The authors are grateful to the National Science Foundation (DMR-1904960, N.L.R.) and the University of Pittsburgh. S.M.-P. acknowledges an Andrew Mellon Predoctoral Fellowship. S.C.B. acknowledges a Dietrich School of Arts and Sciences Fellowship.

Notes

The authors declare no competing financial interest.

■ REFERENCES

- (1) Alivisatos, A. P. (1996) Semiconductor Clusters, Nanocrystals, and Quantum Dots. *Science* 271 (5251), 933–937.
- (2) Nie, Z., Petukhova, A., and Kumacheva, E. (2010) Properties and Emerging Applications of Self-Assembled Structures Made from Inorganic Nanoparticles. *Nat. Nanotechnol.* 5 (1), 15–25.
- (3) Xu, L., Ma, W., Wang, L., Xu, C., Kuang, H., and Kotov, N. A. (2013) Nanoparticle Assemblies: Dimensional Transformation of Nanomaterials and Scalability. *Chem. Soc. Rev.* 42 (7), 3114–3126.
- (4) Laramy, C. R., O'Brien, M. N., and Mirkin, C. A. (2019) Crystal Engineering with DNA. *Nature Reviews Materials* 4 (3), 201–224.
- (5) Fan, Z., and Govorov, A. O. (2010) Plasmonic Circular Dichroism of Chiral Metal Nanoparticle Assemblies. *Nano Lett.* 10 (7), 2580–2587.
- (6) Ben-Moshe, A., Maoz, B. M., Govorov, A. O., and Markovich, G. (2013) Chirality and Chiroptical Effects in Inorganic Nanocrystal Systems with Plasmon and Exciton Resonances. *Chem. Soc. Rev.* 42 (16), 7028–7041.
- (7) Mokashi-Punekar, S., Zhou, Y., Brooks, S. C., and Rosi, N. L. (2019) Construction of Chiral, Helical Nanoparticle Superstructures: Progress and Prospects. *Adv. Mater.*, 1905975.
- (8) Pendry, J. B. (2004) A Chiral Route to Negative Refraction. *Science* 306 (5700), 1353–1355.
- (9) Ma, W., Xu, L., de Moura, A. F., Wu, X., Kuang, H., Xu, C., and Kotov, N. A. (2017) Chiral Inorganic Nanostructures. *Chem. Rev.* 117 (12), 8041–8093.
- (10) Fan, Z., and Govorov, A. O. (2011) Helical Metal Nanoparticle Assemblies with Defects: Plasmonic Chirality and Circular Dichroism. *J. Phys. Chem. C* 115 (27), 13254–13261.

Biochemistry pubs.acs.org/biochemistry Article

- (11) Govorov, A. O., Gun'ko, Y. K., Slocik, J. M., Gérard, V. A., Fan, Z., and Naik, R. R. (2011) Chiral Nanoparticle Assemblies: Circular Dichroism, Plasmonic Interactions, and Exciton Effects. *J. Mater. Chem.* 21 (42), 16806–16818.
- (12) Chen, C.-L., Zhang, P., and Rosi, N. L. (2008) A New Peptide-Based Method for the Design and Synthesis of Nanoparticle Superstructures: Construction of Highly Ordered Gold Nanoparticle Double Helices. *J. Am. Chem. Soc.* 130 (41), 13555–13557.
- (13) Song, C., Zhao, G., Zhang, P., and Rosi, N. L. (2010) Expeditious Synthesis and Assembly of Sub-100 Nm Hollow Spherical Gold Nanoparticle Superstructures. *J. Am. Chem. Soc.* 132 (40), 14033–14035.
- (14) Chen, C.-L., and Rosi, N. L. (2010) Preparation of Unique 1-D Nanoparticle Superstructures and Tailoring Their Structural Features. *J. Am. Chem. Soc.* 132 (20), 6902–6903.
- (15) Hwang, L., Chen, C.-L., and Rosi, N. L. (2011) Preparation of 1-D Nanoparticle Superstructures with Tailorable Thicknesses Using Gold-Binding Peptide Conjugates. *Chem. Commun.* 47 (1), 185–187.
- (16) Song, C., Wang, Y., and Rosi, N. L. (2013) Peptide-Directed Synthesis and Assembly of Hollow Spherical CoPt Nanoparticle Superstructures. *Angew. Chem., Int. Ed.* 52 (14), 3993–3995.
- (17) Song, C., Blaber, M. G., Zhao, G., Zhang, P., Fry, H. C., Schatz, G. C., and Rosi, N. L. (2013) Tailorable Plasmonic Circular Dichroism Properties of Helical Nanoparticle Superstructures. *Nano Lett.* 13 (7), 3256–3261.
- (18) Zhang, C., Song, C., Fry, H. C., and Rosi, N. L. (2014) Peptide Conjugates for Directing the Morphology and Assembly of 1D Nanoparticle Superstructures. *Chem. Eur. J.* 20 (4), 941–945.
- (19) Merg, A. D., Slocik, J., Blaber, M. G., Schatz, G. C., Naik, R., and Rosi, N. L. (2015) Adjusting the Metrics of 1-D Helical Gold Nanoparticle Superstructures Using Multivalent Peptide Conjugates. *Langmuir* 31 (34), 9492–9501.
- (20) Merg, A. D., Boatz, J. C., Mandal, A., Zhao, G., Mokashi-Punekar, S., Liu, C., Wang, X., Zhang, P., van der Wel, P. C. A., and Rosi, N. L. (2016) Peptide-Directed Assembly of Single-Helical Gold Nanoparticle Superstructures Exhibiting Intense Chiroptical Activity. *J. Am. Chem. Soc.* 138 (41), 13655–13663.
- (21) Mokashi-Punekar, S., and Rosi, N. L. (2019) Deliberate Introduction of Particle Anisotropy in Helical Gold Nanoparticle Superstructures. *Part. Part. Syst. Charact.* 36 (5), 1800504.
- (22) Mokashi-Punekar, S., Merg, A. D., and Rosi, N. L. (2017) Systematic Adjustment of Pitch and Particle Dimensions within a Family of Chiral Plasmonic Gold Nanoparticle Single Helices. *J. Am. Chem. Soc.* 139 (42), 15043–15048.
- (23) Mokashi-Punekar, S., Walsh, T. R., and Rosi, N. L. (2019) Tuning the Structure and Chiroptical Properties of Gold Nanoparticle Single Helices via Peptide Sequence Variation. *J. Am. Chem. Soc.* 141 (39), 15710–15716.
- (24) Slocik, J. M., Stone, M. O., and Naik, R. R. (2005) Synthesis of Gold Nanoparticles Using Multifunctional Peptides. *Small 1* (11), 1048–1052.
- (25) Hartgerink, J. D., Beniash, E., and Stupp, S. I. (2001) Self-Assembly and Mineralization of Peptide-Amphiphile Nanofibers. *Science* 294 (5547), 1684–1688.
- (26) Heinz, H., Farmer, B. L., Pandey, R. B., Slocik, J. M., Patnaik, S. S., Pachter, R., and Naik, R. R. (2009) Nature of Molecular Interactions of Peptides with Gold, Palladium, and Pd-Au Bimetal Surfaces in Aqueous Solution. *J. Am. Chem. Soc.* 131 (28), 9704–9714.
- (27) Bedford, N. M., Hughes, Z. E., Tang, Z., Li, Y., Briggs, B. D., Ren, Y., Swihart, M. T., Petkov, V. G., Naik, R. R., Knecht, M. R., and Walsh, T. R. (2016) Sequence-Dependent Structure/Function Relationships of Catalytic Peptide-Enabled Gold Nanoparticles Generated under Ambient Synthetic Conditions. *J. Am. Chem. Soc.* 138 (2), 540–548.
- (28) Cui, H., Cheetham, A. G., Pashuck, E. T., and Stupp, S. I. (2014) Amino Acid Sequence in Constitutionally Isomeric Tetrapeptide Amphiphiles Dictates Architecture of One-Dimensional Nanostructures. *J. Am. Chem. Soc.* 136 (35), 12461–12468.

- (29) Wang, S.-T., Lin, Y., Spencer, R. K., Thomas, M. R., Nguyen, A. I., Amdursky, N., Pashuck, E. T., Skaalure, S. C., Song, C. Y., Parmar, P. A., Morgan, R. M., Ercius, P., Aloni, S., Zuckermann, R. N., and Stevens, M. M. (2017) Sequence-Dependent Self-Assembly and Structural Diversity of Islet Amyloid Polypeptide-Derived β -Sheet Fibrils. ACS Nano 11 (9), 8579–8589.
- (30) Paramonov, S. E., Jun, H.-W., and Hartgerink, J. D. (2006) Self-Assembly of Peptide-Amphiphile Nanofibers: The Roles of Hydrogen Bonding and Amphiphilic Packing. *J. Am. Chem. Soc.* 128 (22), 7291–7298.
- (31) Moyer, T. J., Cui, H., and Stupp, S. I. (2013) Tuning Nanostructure Dimensions with Supramolecular Twisting. *J. Phys. Chem. B* 117 (16), 4604–4610.
- (32) Heinz, H., Farmer, B. L., Pandey, R. B., Slocik, J. M., Patnaik, S. S., Pachter, R., and Naik, R. R. (2009) Nature of Molecular Interactions of Peptides with Gold, Palladium, and Pd-Au Bimetal Surfaces in Aqueous Solution. *J. Am. Chem. Soc.* 131 (28), 9704–9714
- (33) Zanna, N., Milli, L., Del Secco, B., and Tomasini, C. (2016) Factors Affecting the Stabilization of Polyproline II Helices in a Hydrophobic Environment. *Org. Lett.* 18 (7), 1662–1665.
- (34) Barth, A. (2007) Infrared Spectroscopy of Proteins. Biochim. Biophys. Acta, Bioenerg. 1767 (9), 1073-1101.